

# A Novel, Computationally Efficient Multipolar Model Employing Distributed Charges for Molecular Dynamics Simulations

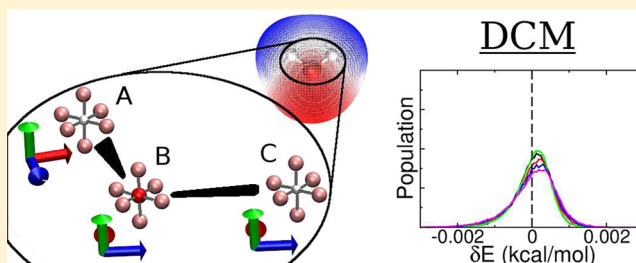
Mike Devereux,<sup>†</sup> Shampa Raghunathan,<sup>†</sup> Dmitri G. Fedorov,<sup>‡</sup> and Markus Meuwly<sup>\*,†</sup>

<sup>†</sup>Universität Basel, Departement Chemie, Klingelbergstrasse 80, CH-4056 Basel, Switzerland

<sup>‡</sup>NRI, National Institute of Advanced Industrial Science and Technology (AIST), 1-1-1 Umezono, Tsukuba, Ibaraki 305-8568, Japan

## S Supporting Information

**ABSTRACT:** A truncated multipole expansion can be re-expressed exactly using an appropriate arrangement of point charges. This means that groups of point charges that are shifted away from nuclear coordinates can be used to achieve accurate electrostatics for molecular systems. We introduce a multipolar electrostatic model formulated in this way for use in computationally efficient multipolar molecular dynamics simulations with well-defined forces and energy conservation in NVE (constant number–volume–energy) simulations. A framework is introduced to distribute torques arising from multipole moments throughout a molecule, and a refined fitting approach is suggested to obtain atomic multipole moments that are optimized for accuracy and numerical stability in a force field context. The formulation of the charge model is outlined as it has been implemented into CHARMM, with application to test systems involving H<sub>2</sub>O and chlorobenzene. As well as ease of implementation and computational efficiency, the approach can be used to provide snapshots for multipolar QM/MM calculations in QM/MM-MD studies and easily combined with a standard point-charge force field to allow mixed multipolar/point charge simulations of large systems.



## INTRODUCTION

Multipolar force fields have been of interest for many years<sup>1–13</sup> due to the additional level of detail that they offer in describing molecular electrostatics over standard point-charge representations.<sup>6</sup> Until recently, however, the extra computational cost associated with the additional terms of the multipole expansion prohibited their use in Molecular Dynamics (MD) simulations for all but the simplest of systems.<sup>14</sup> As available computational power has increased, application to larger systems has become realistic and new multipolar implementations have started to emerge.<sup>10,15</sup> There is still a strong need for accurate and computationally efficient approaches,<sup>16</sup> however—in particular, for complete implementations with all forces analytically included, enabling NVE (constant number–volume–energy) MD simulations for the type of system that has long been accessible to simpler point-charge force fields.<sup>17,18</sup> As few complete multipolar implementations exist, it is not yet fully clear what impact more detailed electrostatics will have on MD simulations, but initial studies have shown that the effect on local dynamics can be important, especially where local interactions are of greater consequence than long time scale conformational sampling of a large system.<sup>7,9,10,14,19</sup> Very long time scale simulations have also recently revealed that current standard point charge force fields routinely used to describe protein systems may not be stable, with proteins slowly drifting away from their experimentally observed structures.<sup>20</sup> A new generation of more detailed force fields may ultimately be required for such applications, despite the increased computational cost.

The approach introduced here for the “Distributed Charge Model” (DCM) is similar in nature to some earlier approaches<sup>21</sup> and directly adapted from recent work of Gao et al.,<sup>22</sup> where a truncated multipole expansion was replaced by an arrangement of seven point charges to apply a multipolar electric field in Fragment Molecular Orbital (FMO) calculations.<sup>23</sup> In DCM, this charge arrangement is modified using spherical harmonics to reduce the number of charges required to six or less, and as no gradients were suggested in the FMO implementation, a framework is introduced to distribute torques arising from these charges throughout a molecule without assuming rigid substructures. The use of point charges reduces the complexity of electrostatic interaction terms relative to a traditional multipolar formalism, yielding efficient MD simulations. A complete description of the derivatives of the electrostatic interaction energy across local axis frames yields energy conservation in NVE MD simulations without the need for short time steps or geometric constraints such as SHAKE. Implementation of the approach into the CHARMM program facilitated integration with the standard CHARMM22 force field, allowing combined DCM/point charge simulations where a single point charge is used per atom for a coarsely described region and several distributed charges are used to describe a region of interest in more detail.

Received: June 12, 2014

Published: August 28, 2014

## METHOD

**DCM.** The starting point for DCM calculations is currently a description of the molecular charge density partitioned into atomic multipole moments. Various schemes exist to perform such partitioning, including Atoms in Molecules<sup>24</sup> and Generalized Distributed Multipole Analysis (GDMA),<sup>25</sup> as well as recent refinement schemes that start with a set of calculated multipole moments and use the electrostatic potential as reference data during fitting to refine them.<sup>26–32</sup> We note that the DCM approach is independent of which scheme is used to obtain atomic multipole moments, but quality of results is limited by the performance of the underlying multipole expansion.

The Cartesian representation of the traceless atomic quadrupole moment tensor is then diagonalized in order to reduce the number of nonzero components to a maximum of three (diagonal) quadrupole terms, three dipole terms, and one charge term and to obtain the associated principal axes.<sup>22,33</sup> The atomic dipole moment is transformed into the same principal axis system. Which eigenvector is assigned as which principal axis is unimportant, as charges are to be transformed into a well-defined local frame (described below).

As noted previously,<sup>34,35</sup> the traceless Cartesian quadrupole moment tensor contains one redundant diagonal term, which can be removed using a spherical harmonic representation. This results in a maximum of six nonzero terms (one charge term, three dipole terms, two quadrupole terms) that can be described exactly by selecting a suitable point charge arrangement. Equations for each multipole of the charge arrangement can then be formulated, expressing for example the total charge as a sum over all individual charges, the total *z*-dipole as the product of each of the charges with its *z*-coordinate and so on for the remaining dipole and quadrupole terms:

$$\begin{aligned} Q_{00} &= \sum_{i=1}^6 q_i & Q_{11s} &= \sum_{i=1}^6 q_i r_{y,i} \\ Q_{10} &= \sum_{i=1}^6 q_i r_{z,i} & Q_{20} &= \sum_{i=1}^6 \frac{1}{2} q_i (3r_{z,i}^2 - r^2) \\ Q_{11c} &= \sum_{i=1}^6 q_i r_{x,i} & Q_{22c} &= \sum_{i=1}^6 \sqrt{\frac{3}{4}} q_i (r_{x,i}^2 - r_{y,i}^2) \end{aligned} \quad (1)$$

$r_{x,i}$  is the *x*-coordinate of charge  $q_i$  for a given charge arrangement. The *x*, *y*, and *z*-coordinates are defined in the frame of the principal axes, and *r* is the distance from the local origin (here the atomic nucleus).

If an arrangement of six charges is chosen with fixed positions, then the six expressions in eq 1 contain six unknown variables corresponding to the atomic charges  $q_i$ . Equation 1 can therefore be treated as a system of six simultaneous equations, solved to find each charge  $q_i$  in terms of the multipole moments  $Q_{lm}$  of rank (*l*, *m*)<sup>34</sup> in the principal axis system. A worked example, where expressions are obtained for the charges of the square pyramidal charge arrangement shown in Figure 1, is shown in section S4 of the Supporting Information.

Without additional constraints, not all charge arrangements yield a uniquely solvable system of equations because, if the charge arrangement is interpreted as a basis set used to describe the atomic multipole moments, it may contain linear dependencies. Of the three examples shown in Figure 1, no general solution is possible for the simultaneous equations corresponding to the trigonal bipyramidal arrangement on the left-hand side, for example, without adjusting the charge positions. The square pyramidal arrangement in the middle of the figure (an

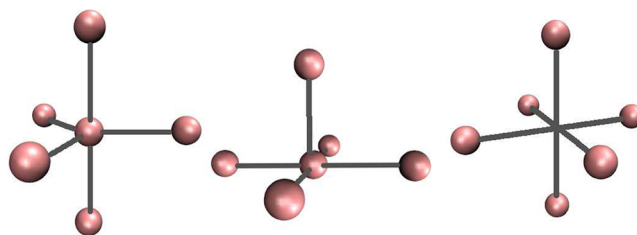


**Figure 1.** Sample charge arrangements for use in the general case where all multipole terms up to quadrupole can be nonzero. The trigonal bipyramidal arrangement (left) has no solution, the octahedral arrangement with one vertex shifted to the center (square pyramidal, middle) leads to larger charges than the purely octahedral arrangement with no central charge (right).

octahedron with one vertex moved to the origin) can be solved (eq 2) and has the advantage that the central charge applies no torque to surrounding atoms, simplifying the expression for its forces and reducing computational overhead. Although charges for this arrangement are larger in magnitude than in the fully octahedral case (eq 3, right-hand side of Figure 1), which could affect numerical stability of simulations in extreme cases due to loss of precision, the value of  $d_q$  may be increased to decrease the size of the charges.

The pyramidal (eq 2) and octahedral (eq 3) charge distributions are expressed as

$$\begin{aligned} q_{(d_q,0,0)} &= \frac{\frac{1}{2}d_q(Q_{11s} + Q_{11c}) + \frac{\sqrt{3}}{3}Q_{22c}}{d_q^2} \\ q_{(0,0,d_q)} &= \frac{\frac{1}{2}d_q(Q_{11s} + Q_{10}) + \frac{1}{2}Q_{20} + \frac{\sqrt{3}}{6}Q_{22c}}{d_q^2} \\ q_{(-d_q,0,0)} &= \frac{\frac{1}{2}d_q(Q_{11s} - Q_{11c}) + \frac{\sqrt{3}}{3}Q_{22c}}{d_q^2} \\ q_{(0,0,-d_q)} &= \frac{\frac{1}{2}d_q(Q_{11s} - Q_{10}) + \frac{1}{2}Q_{20} + \frac{\sqrt{3}}{6}Q_{22c}}{d_q^2} \\ q_{(0,d_q,0)} &= \frac{Q_{11s}}{d_q} & q_{(0,0,0)} &= Q_{00} - \sum_{i=1}^5 q_i \end{aligned} \quad (2)$$

$$\begin{aligned} q_{(d_q,0,0)} &= \frac{Q_{00}}{6} + \frac{Q_{11c}}{2d_q} - \frac{Q_{20}}{6d_q^2} + \frac{Q_{22c}}{2\sqrt{3}d_q^2} \\ q_{(0,-d_q,0)} &= \frac{Q_{00}}{6} - \frac{Q_{11s}}{2d_q} - \frac{Q_{20}}{6d_q^2} - \frac{Q_{22c}}{2\sqrt{3}d_q^2} \\ q_{(-d_q,0,0)} &= \frac{Q_{00}}{6} - \frac{Q_{11c}}{2d_q} - \frac{Q_{20}}{6d_q^2} + \frac{Q_{22c}}{2\sqrt{3}d_q^2} \\ q_{(0,0,d_q)} &= \frac{Q_{00}}{6} + \frac{Q_{10}}{2d_q} + \frac{Q_{20}}{3d_q^2} \\ q_{(0,d_q,0)} &= \frac{Q_{00}}{6} + \frac{Q_{11s}}{2d_q} - \frac{Q_{20}}{6d_q^2} - \frac{Q_{22c}}{2\sqrt{3}d_q^2} \\ q_{(0,0,-d_q)} &= \frac{Q_{00}}{6} - \frac{Q_{10}}{2d_q} + \frac{Q_{20}}{3d_q^2} \end{aligned} \quad (3)$$

where  $q_{(d_q,0,0)}$  is a charge lying along the  $x$  principal-axis,  $q_{(-d_q,0,0)}$  lies along negative  $x$ . The parameter  $d_q$  defines the distance of each charge from the origin. Any charge arrangement with nonzero  $d_q$  will exhibit nonzero higher order multipole terms (in this case octupole moments and beyond). A small value of  $d_q$  means that these terms have negligible impact on the electrostatic potential generated outside the atom, but if  $d_q$  is too small then charges will become large according to eqs 2 and 3. The value of  $d_q = 0.25 a_0$  suggested by Gao et al.<sup>22</sup> was found to be suitable in many cases and is adopted here unless otherwise stated. We note, however, that  $d_q$  offers an additional degree of freedom that can be leveraged to deliberately introduce higher-order multipole moments and improve the accuracy of the DCM arrangement beyond that of the underlying truncated multipole expansion. There is no requirement for  $d_q$  to be the same for all charges.

Finally, diagonalization of the quadrupole tensor provides an efficient means to leverage symmetry and reduce the number of nonzero multipole components at the atomic level, but further gains are possible by repartitioning the molecular electron density between atoms in such a way that certain atoms receive vanishing multipole moments. One such reduced multipolar description for water was identified in previous work by Lee et al.<sup>36</sup> based on GDMA calculations, where H atoms were left with only a charge term and O exhibited a charge,  $Q_{10}$  dipole term, and  $Q_{20}$  and  $Q_{22c}$  quadrupole terms. An equivalent DCM charge arrangement was found, with one charge at each H atom nuclear position and 4 DCM charges for oxygen, by solving the corresponding system of simultaneous equations for the smaller charge arrangement. The set of simultaneous equations to be solved is again expanded in the Supporting Information in section S4. The oxygen charges and their positions in the principal axis system were calculated to be

$$\begin{aligned} q_{(0,d_2,d_1)} &= \frac{Q_{00}}{4} + \frac{\sqrt{3}}{24} \frac{Q_{00}Q_{22c}}{Q_{20}} + \frac{\sqrt{3}}{16} \frac{Q_{00}Q_{10}^2f}{Q_{20}Q_{22c}} \\ q_{(0,-d_2,d_1)} &= \frac{Q_{00}}{4} + \frac{\sqrt{3}}{24} \frac{Q_{00}Q_{22c}}{Q_{20}} + \frac{\sqrt{3}}{16} \frac{Q_{00}Q_{10}^2f}{Q_{20}Q_{22c}} \\ q_{(d_2,0,-d_1)} &= \frac{Q_{00}}{4} - \frac{\sqrt{3}}{24} \frac{Q_{00}Q_{22c}}{Q_{20}} - \frac{\sqrt{3}}{16} \frac{Q_{00}Q_{10}^2f}{Q_{20}Q_{22c}} \\ q_{(-d_2,0,-d_1)} &= \frac{Q_{00}}{4} - \frac{\sqrt{3}}{24} \frac{Q_{00}Q_{22c}}{Q_{20}} - \frac{\sqrt{3}}{16} \frac{Q_{00}Q_{10}^2f}{Q_{20}Q_{22c}} \end{aligned} \quad (4)$$

$$d_1 = -\frac{\sqrt{3}}{6} \frac{Q_{22c}}{Q_{10}} + \frac{\sqrt{3}}{4} \frac{Q_{10}f}{Q_{22c}} \quad (5)$$

$$d_2 = -\frac{1}{2} \sqrt{\frac{4}{3} \frac{Q_{22c}^2}{Q_{10}^2} - 2f} \quad (6)$$

$$f = \sqrt{\frac{16}{3} \frac{Q_{20}Q_{22c}^2}{Q_{00}Q_{10}^2} + \frac{4}{9} \frac{Q_{22c}^4}{Q_{10}^4}} \quad (7)$$

where  $f$  is a common factor. Charges  $q$  are arranged in a distorted tetrahedron, where the position vector components  $d_1$  and  $d_2$  along the principal axes change according to eqs 5 and 6 (Figure 2). For oxygen in water, the geometry becomes almost planar. Although the distance  $d_q$  from the nucleus is no longer flexible for

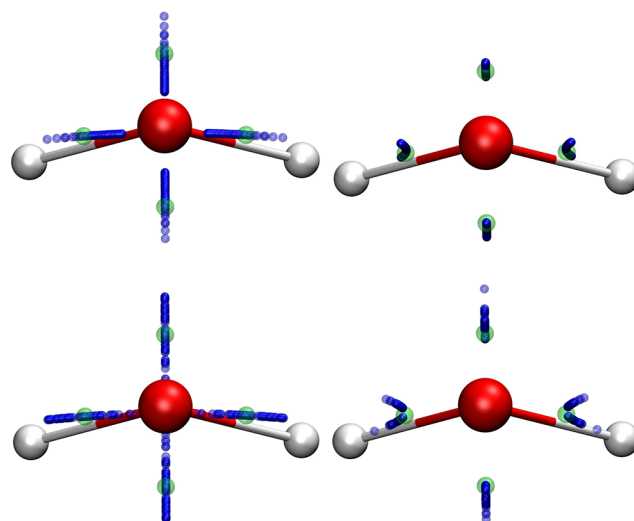


**Figure 2.** DCM charge positions for oxygen atom in H<sub>2</sub>O using 4-charge model. Green spheres show DCM charge coordinates corresponding to multipole moments of Lee et al.<sup>36</sup> Blue spheres show how coordinates change as a function of atomic charge  $Q_{00}$  between  $-0.14$  and  $-0.98$  au (top-left),  $z$ -dipole  $Q_{10}$  between  $1.0$  and  $-1.0$  au (top-right), quadrupole  $Q_{20}$  between  $0.06$  and  $0.00$  au (bottom-left), and quadrupole  $Q_{22c}$  between  $0.97$  and  $-0.99$  au (bottom-right). No points exceed  $0.66$  Å from the oxygen nucleus.

this solution, as it was in the octahedral and pyramidal cases, a significant gain in computational efficiency is expected by reducing the number of DCM charges on oxygen from 6 to 4. A DCM model equivalent to the multipolar model of Lee et al. can thus be achieved using one charge for each H atom and four charges for O, at the cost of a possible increase in the octupole moment in atoms where  $d_q$  becomes large.

**Local Frames.** After obtaining positions and magnitudes of charges relative to the principal axes of the Cartesian quadrupole moment tensor, a local molecular frame must be defined to place the charges relative to the surrounding nuclei. While different schemes are possible, the approach adopted here is to divide each molecule into groups of three noncolinear atoms. The three atoms provide two bond vectors, which are sufficient to define a plane and corresponding axis system for each atom (Figure 3).

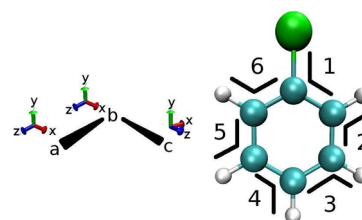


**Figure 3.** Division of chlorobenzene into six local frames made up of groups of three noncolinear atoms (right), and the local axis system for each atom in each frame (left). Local  $z$ -axes,  $\hat{e}_z$ , (blue axes in the figure) are defined as  $\mathbf{r}_{ba}/\|\mathbf{r}_{ba}\|$  for atoms  $a$  and  $b$  and  $\mathbf{r}_{bc}/\|\mathbf{r}_{bc}\|$  for atom  $c$ . The local  $y$ -axis,  $\hat{e}_y$ , (green axes in the figure) is the normalized cross product  $(\hat{e}_{z,a} \times \hat{e}_{z,c})/(\|\hat{e}_{z,a} \times \hat{e}_{z,c}\|)$  for  $a$ ,  $b$ , and  $c$ . The local  $x$ -axis,  $\hat{e}_x$ , (red axes in the figure) is the cross product  $\hat{e}_{z,a} \times \hat{e}_y$  for  $a$  and  $b$  and  $\hat{e}_{z,c} \times \hat{e}_y$  for  $c$ .

Alternative frames involving, for example, the bisector of  $\mathbf{r}_{ba}$  and  $\mathbf{r}_{bc}$  to define the  $z$ -axis unit vector  $\hat{e}_z$  for atom  $b$  could also be considered,<sup>27,37</sup> for the special case where the principal axes move relative to the bond bisector as a function of change in valence angle, rather than any of the bond vectors. This system is

not necessary for chlorobenzene, where principal axes will tend to move relative to a bond vector, or in H<sub>2</sub>O, where SHAKE<sup>38</sup> is generally applied to constrain the HOH angle. Where atoms appear in more than one local frame, for example the carbon atoms in Figure 1, DCM charges for that atom are assigned to one of the frames only and are zeroed in all others. This framework is general and can be applied to any molecular system where there are at least three noncolinear atoms.

DCM charges, initially defined relative to the principal axes, are transformed to the local axis system of each atom so that they can be placed for any orientation of the atoms of the local frame. Considering a charge  $q$  with coordinates  $u\hat{\mathbf{p}}_x$ ,  $v\hat{\mathbf{p}}_y$ , and  $w\hat{\mathbf{p}}_z$ , where  $\hat{\mathbf{p}}_x$ ,  $\hat{\mathbf{p}}_y$ , and  $\hat{\mathbf{p}}_z$  are the principal axes of the quadrupole moment tensor, the coordinates  $u'\hat{\mathbf{e}}_x$ ,  $v'\hat{\mathbf{e}}_y$ , and  $w'\hat{\mathbf{e}}_z$  in the local atomic frame are obtained from the following transformation:

$$\begin{aligned} u' &= u\hat{\mathbf{p}}_x \cdot \hat{\mathbf{e}}_x + v\hat{\mathbf{p}}_y \cdot \hat{\mathbf{e}}_x + w\hat{\mathbf{p}}_z \cdot \hat{\mathbf{e}}_x \\ v' &= u\hat{\mathbf{p}}_x \cdot \hat{\mathbf{e}}_y + v\hat{\mathbf{p}}_y \cdot \hat{\mathbf{e}}_y + w\hat{\mathbf{p}}_z \cdot \hat{\mathbf{e}}_y \\ w' &= u\hat{\mathbf{p}}_x \cdot \hat{\mathbf{e}}_z + v\hat{\mathbf{p}}_y \cdot \hat{\mathbf{e}}_z + w\hat{\mathbf{p}}_z \cdot \hat{\mathbf{e}}_z \end{aligned} \quad (8)$$

The electrostatic interaction energy between atom a in frame 1 and atom d in frame 2 (Figure 4) is

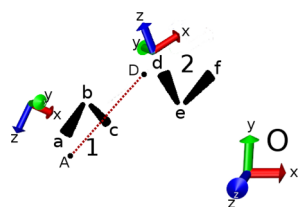


**Figure 4.** Interaction between charge A associated with atom a in frame 1 and charge D associated with atom d in frame 2. The local axes  $\hat{\mathbf{e}}_x$ ,  $\hat{\mathbf{e}}_y$ , and  $\hat{\mathbf{e}}_z$  for atoms a and d are shown relative to the global axis and global origin O. Atoms b and c are the neighbors making up frame 1 with atom a, atoms e and f make up frame 2 with atom d.

$$\begin{aligned} V(\mathbf{R}_a, \mathbf{R}_b, \mathbf{R}_c, \mathbf{R}_d, \mathbf{R}_e, \mathbf{R}_f) \\ = \sum_{m=1}^{N_a} \sum_{n=1}^{N_d} \frac{q_{a,m} q_{d,n}}{\|\mathbf{R}_{q_{a,m}}(\mathbf{R}_a, \mathbf{R}_b, \mathbf{R}_c) - \mathbf{R}_{q_{d,n}}(\mathbf{R}_d, \mathbf{R}_e, \mathbf{R}_f)\|} \end{aligned} \quad (9)$$

$$\mathbf{R}_{q_{a,m}}(\mathbf{R}_a, \mathbf{R}_b, \mathbf{R}_c) = \begin{pmatrix} \mathbf{R}_{a,x} + u'_m \hat{\mathbf{e}}_{x,i} + v'_m \hat{\mathbf{e}}_{y,i} + w'_m \hat{\mathbf{e}}_{z,i} \\ \mathbf{R}_{a,y} + u'_m \hat{\mathbf{e}}_{x,j} + v'_m \hat{\mathbf{e}}_{y,j} + w'_m \hat{\mathbf{e}}_{z,j} \\ \mathbf{R}_{a,z} + u'_m \hat{\mathbf{e}}_{x,k} + v'_m \hat{\mathbf{e}}_{y,k} + w'_m \hat{\mathbf{e}}_{z,k} \end{pmatrix} \quad (10)$$

where  $\mathbf{R}_a$ ,  $\mathbf{R}_b$ , and  $\mathbf{R}_c$  are the position vectors of atoms a, b, and c used to define frame 1.  $\mathbf{R}_d$ ,  $\mathbf{R}_e$ , and  $\mathbf{R}_f$  similarly define frame 2.  $N_a$  is the number of DCM charges assigned to atom a in frame 1.  $\mathbf{R}_{q_{a,m}}(\mathbf{R}_a, \mathbf{R}_b, \mathbf{R}_c)$  is the position vector of the  $m^{\text{th}}$  DCM charge  $q$  on atom a (eq 10). As indicated, the position of each DCM charge is a function of the coordinates of the three atoms that define its local axes  $\hat{\mathbf{e}}_x$ ,  $\hat{\mathbf{e}}_y$ ,  $\hat{\mathbf{e}}_z$ . The one exception is when a DCM charge is at the local origin (atomic nucleus), where  $u' = v' = w' = 0$ , and the charge is a function of only one nuclear coordinate.  $u'$ ,  $v'$ , and  $w'$  are defined in eq 8.  $\hat{\mathbf{e}}_{z,j}$  is the  $j$  component of local frame vector  $\hat{\mathbf{e}}_z$  in the global axis.  $\mathbf{R}_{q_{d,n}}(\mathbf{R}_d, \mathbf{R}_e, \mathbf{R}_f)$  is defined analogously to  $\mathbf{R}_{q_{a,m}}(\mathbf{R}_a, \mathbf{R}_b, \mathbf{R}_c)$  (eq 10).

The derivatives for a Coulomb interaction between two point charges  $q$  placed at the nuclear positions of atoms a and d follow the familiar relationship:

$$\frac{\partial V}{\partial R_{a,\alpha}} = - \frac{R_{a,d,\alpha} q_a q_d}{r_{ad}^3} \quad (11)$$

where  $R_{a,\alpha}$  is the  $\alpha = x, y$ , or  $z$  component of the position vector of nucleus a,  $r_{ad}$  is the internuclear separation and  $R_{a,d,\alpha}$  is the  $\alpha$  component of the internuclear separation vector  $\mathbf{R}_{ad}$ . Any DCM charges placed at the nuclear position use exactly these expressions for the energy and derivatives. DCM charges on atom a that are shifted from the nuclear position will exert an additional force on the other two atoms b and c that are used to define a's local axis system (Figure 4). This is because any change in the position of atoms b and c can rotate the local axis system of a and with it the DCM charges that are placed relative to its nucleus, even though the nuclear coordinates of a are unaffected. The derivatives of the interaction between a charge A on atom a in frame 1 (one particular index ' $m$ ' in eq 9) and a charge D on atom d in frame 2 are then described as

$$\begin{aligned} \frac{\partial V}{\partial R_{a,\alpha}} = \\ - \frac{q_A q_D (R_{AD,x}(\hat{\alpha} \cdot \hat{\mathbf{x}} + g_{1\alpha}) + R_{AD,y}(\hat{\alpha} \cdot \hat{\mathbf{y}} + g_{2\alpha}) + R_{AD,z}(\hat{\alpha} \cdot \hat{\mathbf{z}} + g_{3\alpha}))}{r_{AD}^3} \end{aligned} \quad (12)$$

$$\frac{\partial V}{\partial R_{b,\alpha}} = - \frac{q_A q_D (R_{AD,x} g_{4\alpha} + R_{AD,y} g_{5\alpha} + R_{AD,z} g_{6\alpha})}{r_{AD}^3} \quad (13)$$

$$\frac{\partial V}{\partial R_{c,\alpha}} = - \frac{q_A q_D (R_{AD,x} g_{7\alpha} + R_{AD,y} g_{8\alpha} + R_{AD,z} g_{9\alpha})}{r_{AD}^3} \quad (14)$$

where the scalar product  $\hat{\alpha} \cdot \hat{\mathbf{x}}$  is simply 1 when  $\alpha = x$  and zero otherwise.  $R_{AD,x}$  is the  $x$ -component of the vector  $\mathbf{R}_{AD}$  from charge A to charge D. The coefficients  $g_{1\alpha}$  to  $g_{9\alpha}$  contain the partial derivatives of the local unit vectors of the frame ( $\hat{\mathbf{e}}_x$ ,  $\hat{\mathbf{e}}_y$ ,  $\hat{\mathbf{e}}_z$ , eq 8) with respect to the nuclear coordinates  $R_{a,\alpha}$ ,  $R_{b,\alpha}$ , and  $R_{c,\alpha}$ . These coefficients (eqs 15–23) are the same for all interactions involving charge A and are calculated once for each simulation time step according to

$$g_{1\alpha} = u' \frac{\partial \hat{\mathbf{e}}_{x,i}}{\partial R_{a,\alpha}} + v' \frac{\partial \hat{\mathbf{e}}_{y,i}}{\partial R_{a,\alpha}} + w' \frac{\partial \hat{\mathbf{e}}_{z,i}}{\partial R_{a,\alpha}} \quad (15)$$

$$g_{2\alpha} = u' \frac{\partial \hat{\mathbf{e}}_{x,j}}{\partial R_{a,\alpha}} + v' \frac{\partial \hat{\mathbf{e}}_{y,j}}{\partial R_{a,\alpha}} + w' \frac{\partial \hat{\mathbf{e}}_{z,j}}{\partial R_{a,\alpha}} \quad (16)$$

$$g_{3\alpha} = u' \frac{\partial \hat{\mathbf{e}}_{x,k}}{\partial R_{a,\alpha}} + v' \frac{\partial \hat{\mathbf{e}}_{y,k}}{\partial R_{a,\alpha}} + w' \frac{\partial \hat{\mathbf{e}}_{z,k}}{\partial R_{a,\alpha}} \quad (17)$$

$$g_{4\alpha} = u' \frac{\partial \hat{\mathbf{e}}_{x,i}}{\partial R_{b,\alpha}} + v' \frac{\partial \hat{\mathbf{e}}_{y,i}}{\partial R_{b,\alpha}} + w' \frac{\partial \hat{\mathbf{e}}_{z,i}}{\partial R_{b,\alpha}} \quad (18)$$

$$g_{5\alpha} = u' \frac{\partial \hat{\mathbf{e}}_{x,j}}{\partial R_{b,\alpha}} + v' \frac{\partial \hat{\mathbf{e}}_{y,j}}{\partial R_{b,\alpha}} + w' \frac{\partial \hat{\mathbf{e}}_{z,j}}{\partial R_{b,\alpha}} \quad (19)$$

$$g_{6\alpha} = u' \frac{\partial \hat{\mathbf{e}}_{x,k}}{\partial R_{b,\alpha}} + v' \frac{\partial \hat{\mathbf{e}}_{y,k}}{\partial R_{b,\alpha}} + w' \frac{\partial \hat{\mathbf{e}}_{z,k}}{\partial R_{b,\alpha}} \quad (20)$$



$$g_{7\alpha} = u' \frac{\partial \hat{\mathbf{e}}_{x,i}}{\partial R_{c,\alpha}} + v' \frac{\partial \hat{\mathbf{e}}_{y,i}}{\partial R_{c,\alpha}} + w' \frac{\partial \hat{\mathbf{e}}_{z,i}}{\partial R_{c,\alpha}} \quad (21)$$

$$g_{8\alpha} = u' \frac{\partial \hat{\mathbf{e}}_{x,j}}{\partial R_{c,\alpha}} + v' \frac{\partial \hat{\mathbf{e}}_{y,j}}{\partial R_{c,\alpha}} + w' \frac{\partial \hat{\mathbf{e}}_{z,j}}{\partial R_{c,\alpha}} \quad (22)$$

$$g_{9\alpha} = u' \frac{\partial \hat{\mathbf{e}}_{x,k}}{\partial R_{c,\alpha}} + v' \frac{\partial \hat{\mathbf{e}}_{y,k}}{\partial R_{c,\alpha}} + w' \frac{\partial \hat{\mathbf{e}}_{z,k}}{\partial R_{c,\alpha}} \quad (23)$$

where  $u'$ ,  $v'$ , and  $w'$  are again as defined in eq 8.  $\hat{\mathbf{e}}_{x,i}$  is the  $i$ -component of the local  $\hat{\mathbf{e}}_x$  axis vector in the global frame;  $R_{a,\alpha}$  is the  $\alpha = x, y, z$  component of the position vector of atom  $a$ .

**Computational Efficiency.** The computational efficiency of the implementation can be explored by breaking down the interaction energy and forces into components that must be evaluated only once for a given molecule, components that must be re-evaluated each time the molecular coordinates change (once per time step in an MD simulation), and components that must be re-evaluated for every charge–charge interaction.

The charges and their positions in the local frame (eqs 2 and 3) are fixed parameters that must be evaluated once only. The magnitudes of the charges are not conformation-dependent in the current implementation, so they do not require re-evaluation at run-time. The local axes  $\hat{\mathbf{e}}_x$ ,  $\hat{\mathbf{e}}_y$ , and  $\hat{\mathbf{e}}_z$  and hence the positions of the charges in the global axis system (eq 10) are evaluated once per time step for each frame. These terms scale with the number of frames in the system and the number of atoms,  $N$ . By far the most time-consuming step in the evaluation of the electrostatic energy is therefore eq 9, the charge–charge Coulomb interaction energy, which must be evaluated for every charge–charge interaction. In the simplest case, where all atoms are assigned the same number of DCM charges “ $n$ ”, evaluation of the Coulomb interaction energy term will scale with  $0.5n^2N(N-1)$ , a factor of  $n^2$  slower than a standard point charge representation with only one charge at the nuclear position. Any redundancy involved in choosing overlapping local frames (Figure 3) therefore has relatively little impact on overall computational cost.

The derivatives of the energy (forces) can be broken down into similar components, and computational cost is again dominated by the Coulomb term (eqs 11–14). The computational cost of evaluating the many coefficients in eqs 15–23 is therefore small in comparison to the time spent evaluating eqs 12–14, despite the fact that the coefficient terms are more complex. These equations show that the additional overhead  $t_d$  for the derivatives per off-center DCM charge–charge interaction is equal to nine times the time taken to evaluate eq 14 ( $\alpha = x, y, z$  for atoms  $a, b$ , and  $c$  that define atom  $a$ 's frame). The Coulomb term from eq 11 is evaluated only once per charge–charge interaction, meaning that each of the nine terms contributing to  $t_d$  is a simple sum of three products. Assuming the worst case with the same number of DCM charges on every atom, none of which are at the nuclear coordinate, an evaluation of the electrostatic forces using the DCM model is therefore expected to be a factor of  $n^2 t_d$  slower than the same energy evaluation in a standard point charge force field. In practice, considerable savings are possible by exploiting any vanishing multipole moments that arise due to symmetry in the partitioned molecular electron density or by repartitioning the molecular electron density, and also by using the nuclear coordinate for one of the charges wherever possible.

As a comparison, a standard multipolar force field employing diagonalized quadrupole moment tensors would also require  $n^2$

terms per atom–atom interaction, assuming the same maximum atomic multipolar rank on each atom, where  $n$  is now the number of nonzero multipole components. In the general case where all multipole moments are nonzero  $n = 6$  (1 charge term, 3 dipole terms and 2 quadrupole terms). The interaction between two atoms,  $a$  and  $d$  therefore requires 36 interaction terms, detailed in eqs 24–32.<sup>34</sup>

$$V_{Q_{00,a}Q_{1m,d}} = \frac{Q_{00,a}Q_{1m,d}r_{ad}^a}{r_{ad}^2} \quad (24)$$

$$V_{Q_{1m,a}Q_{1m,d}} = \frac{Q_{1m,a}Q_{1m,d}(3r_{\alpha}^a r_{\beta}^d + c_{\alpha,\beta})}{r_{ad}^3} \quad (25)$$

$$V_{Q_{20,a}Q_{00,d}} = \frac{Q_{20,a}Q_{00,d}(3r_z^{a2} - 1)}{2r_{ad}^3} \quad (26)$$

$$V_{Q_{22c,a}Q_{00,d}} = \frac{\sqrt{3}Q_{22c,a}Q_{00,d}(r_x^{a2} - r_y^{a2})}{2r_{ad}^3} \quad (27)$$

$$V_{Q_{20,a}Q_{1m,d}} = \frac{Q_{20,a}Q_{1m,d}(15r_z^{a2}r_{\beta}^d + 6c_{z,\beta}r_{\alpha}^a - 3r_{\beta}^d)}{2r_{ad}^4} \quad (28)$$

$$V_{Q_{22c,a}Q_{1m,d}} = \frac{\sqrt{3}Q_{22c,a}Q_{1m,d}(5r_{\beta}^d(r_x^{a2} - r_y^{a2}) + 2c_{x,\beta}r_{\alpha}^a - 2c_{y,\beta}r_{\alpha}^a)}{2r_{ad}^4} \quad (29)$$

$$V_{Q_{20,a}Q_{20,d}} = \frac{3Q_{20,a}Q_{20,d}(35r_z^{a2}r_z^{d2} - 5r_z^{a2} - 5r_z^{d2} + 20r_z^a r_z^d c_{z,z} + 2c_{z,z}^2 + 1)}{4r_{ad}^5} \quad (30)$$

$$V_{Q_{20,a}Q_{22c,d}} = (\sqrt{3}Q_{20,a}Q_{22c,d}(35r_z^{a2}r_x^d r_y^d - 5r_x^d r_y^d + 10r_z^a r_x^d c_{y,z} + 10r_z^a r_y^d c_{z,x} + 2c_{z,x}c_{z,y})) / 2r_{ad}^5 \quad (31)$$

$$V_{Q_{22c,a}Q_{22c,d}} = \frac{1}{4}Q_{22c,a}Q_{22c,d}(35r_x^{a2}r_x^{d2} - 35r_x^{a2}r_y^d r_y^d - 35r_y^{a2}r_x^d r_x^d + 35r_y^{a2}r_y^d r_y^d + 20r_x^a r_x^d c_{x,x} - 20r_x^a r_y^d c_{x,y} - 20r_y^a r_x^d c_{y,x} + 20r_y^a r_y^d c_{y,y} + 2c_{x,x}^2 - 2c_{x,y}^2 - 2c_{y,x}^2 + 2c_{y,y}^2)r_{ad}^{-5} \quad (32)$$

Here, the multipole moment  $Q_{lm}$  is the dipole moment component  $m$ . When  $m = 0, 1c, 1s, \alpha = z, x, y$  respectively.  $r_{ad}$  is the internuclear separation of atoms  $a$  and  $d$ ,  $r_{\alpha}^a$  is defined as the scalar product  $\hat{\mathbf{e}}_{\alpha}^a \cdot \hat{\mathbf{e}}_{\alpha}^d$  where  $\hat{\mathbf{e}}_{\alpha}^a$  is a unit vector along the  $\alpha$  axis of atom  $a$  ( $\alpha = x, y, z$ ).  $\hat{\mathbf{e}}_{\alpha}^d$  is a unit vector in the direction from  $a$  to  $d$ .  $\beta = x, y, z$  for atom  $d$ ,  $c_{\alpha,\beta}$  is the scalar product  $\hat{\mathbf{e}}_{\alpha}^a \cdot \hat{\mathbf{e}}_{\beta}^d$ . There is clearly significant additional complexity in these interaction terms when compared to the purely Coulombic terms of DCM interactions (eq 9), making DCM more straightforward to implement into molecular dynamics code. However, the multipole expansion has the advantage that whereas the vector  $\mathbf{r}_{AD}$  between two DCM charges changes and needs to be re-evaluated for every pair of charges on atoms  $a$  and  $d$ , the origin of the multipole expansion is fixed and the interaction vector and its magnitude must be calculated only once per atom–atom pair. Initial investigation has shown that the DCM algorithm compares favorably with a multipolar algorithm currently implemented in CHARMM<sup>29</sup> in

terms of computational cost, but any comparison will depend on the details of the implementation involved.

**Computational Details.** Optimized monomer geometries, electron densities, and reference electrostatic potential energies were calculated using the Gaussian09 suite of programs<sup>39</sup> with B3LYP and an aug-cc-pVQZ basis set for H<sub>2</sub>O. The larger chlorobenzene molecule was first optimized at the B3LYP/6-311+G(2d,p) level, then a B3LYP/aug-cc-pVTZ single point calculation was used to obtain the electron density and reference electrostatic potential energy values.

Multipole moments were obtained using both GDMA<sup>25</sup> and a multipolar fitting scheme adapted from earlier work.<sup>26–32</sup> For the latter, the electrostatic potential energy across a grid of points outside the 0.001 au isodensity surface is used as reference data and the multipole moments are treated as adjustable parameters. The I-NoLLS<sup>40</sup> Interactive Nonlinear Least Squares fitting program was used, the total molecular charge, dipole, and quadrupole were constrained to their reference values as described in ref 26. At the B3LYP/aug-cc-pVQZ level of theory (used previously),<sup>19</sup> the molecular dipole moment was found to be 0.73 au and the molecular quadrupole moment was 2.13 au. It would also be possible to constrain to the experimentally observed bulk water dipole moment, although this may affect agreement with the calculated gas-phase electrostatic potential used for fitting atomic multipole moments. Symmetry constraints were also applied, so that atoms that are linked via symmetry received equivalent multipole moments. A new adaptation was introduced whereby all multipoles are initially set to zero and soft constraints are applied to bias their values toward zero during fitting. The constraints ensure that the total molecular moments remain at reference values by sharing atomic corrections equally between all atoms, and the final fitted multipoles represent a solution, which has optimally converged by multipolar rank 2 (atomic quadrupole moments), that implicitly attempts to reduce short-range “penetration” errors where the multipole expansion breaks down and that favors small values of atomic multipole moments to improve stability of the model during simulations.

DCM electrostatic interaction energies of water dimers were calculated using a newly implemented in-house DCM module for CHARMM and using the MTPL module of Bereau et al. for comparison with truncated multipole expansions.<sup>29</sup> To provide ab initio reference data, Reduced Variational Space (RVS) energy decomposition analysis<sup>41</sup> was performed on each water dimer at the Restricted Hartree–Fock (RHF) level of theory with aug-cc-pVQZ basis set to evaluate the exact Coulomb integral over the gas-phase charge densities of the monomers. The GAMESS<sup>42</sup> program was used for RVS analysis with basis set taken from the Basis Set Exchange.<sup>43</sup> The current RVS implementation in GAMESS cannot be used with DFT or other correlated methods.

500 ps NVE MD simulations of the water trimer were performed at 50 K, also with DCM implemented in the CHARMM program. Geometries were optimized, heated from 0 K to the specified simulation temperature, and equilibrated during a short NVT simulation, and then, trajectories were generated without a thermostat in an NVE ensemble. A relatively large 1 fs time step was used despite not applying SHAKE constraints to demonstrate computational stability and energy conservation during the simulations. Fitting of remaining force field terms is not examined in the current work, so bonded and Lennard-Jones nonbonded parameters for DCM water molecules were taken from the TIP3P parametrization.<sup>44</sup>

A similar approach was used for a benchmarking simulation of a droplet containing 130 water molecules. This time a more standard 0.25 fs time step was used, again without SHAKE constraints in a short 0.75 ps simulation. A standard quartic restraining potential in CHARMM was found to cause energy drift during NVE simulations, so an alternative spherical restraining potential with no discontinuity in the associated forces was implemented and applied to water molecule oxygen atoms:

$$V(r) = \left( \epsilon \frac{r^2}{r_{\text{cut}}^2} \right)^{10} \quad (33)$$

where  $r$  is the distance from the atom to the global origin,  $\epsilon$  is a scaling factor set to 0.1, and  $r_{\text{cut}}$  is the radius of the sphere, in this case 10 Å. A 10 Å sphere of water molecules was created, optimized with the adopted basis Newton–Raphson algorithm in CHARMM, then heated to 300 K over 12.5 ps (50,000 time steps). After 20 ps of NVT equilibration, the final 0.75 ps benchmarking NVE trajectories were performed using different charge models. Remaining bonded and nonbonded terms were as for the water trimer.

A larger water droplet containing a core of 42 DCM water molecules and an outer shell of 327 TIP3P water molecules was created by overlaying a 14 Å sphere of TIP3P water molecules onto a 7 Å sphere of DCM water molecules. A spherical restraining potential with  $r_{\text{cut}} = 15$  Å (eq 33) was applied to all TIP3P oxygen atoms; a potential with radius  $r_{\text{cut}} = 8$  Å was applied to the DCM water molecule O atoms. This system was minimized, heated, and equilibrated as for the water sphere described above. The four-charge DCM model (eqs 4–7) was used for the core water molecules, and two types of NVE-continuations were considered: 75 ps without SHAKE and a time step of 0.25 fs, and 300 ps with SHAKE applied and a time step of 1 fs.

Finally, a chlorobenzene molecule was solvated in a water droplet with radius 11 Å. A pyramidal DCM charge model with  $d_q = 0.25 a_0$  was used for water and chlorobenzene atoms. Missing bonded and nonbonded parameters for chlorobenzene were taken from a test set generated with the CGenFF tool by MacKerell and co-workers.<sup>45</sup> A total of 171 water molecules were included in the system and a spherical restraining potential with radius  $r_{\text{cut}} = 11.5$  Å was applied to water oxygen atoms. Reference simulations used TIP3P charges for water and CGenFF charges for chlorobenzene. Remaining simulation details were as for the previous systems, again with 75 ps (300000 0.25 fs time steps) NVE production runs without SHAKE constraints or 300 ps (300000 1 fs time steps) with SHAKE applied to H atoms.

## RESULTS AND DISCUSSION

**Multipole Fitting.** Fitting of the H<sub>2</sub>O multipole moments to electrostatic potential energy (ESP) values used a sparse 3D grid with 2373 points across the volume outside the 0.001 au isodensity surface. The dependence of the error in ESP across the grid on adjustable multipole moments was found to be linear, and so, fitting converged with a single iteration to yield the values shown on the right-hand side of Table 1. For comparison, GDMA multipole moments calculated at the same level of theory as the ESP data are included on the left-hand side of the table. Loosely constraining all atomic multipole components to zero kept fitted multipole moment components smaller than their GDMA counterparts, while still maintaining the total molecular multipole moments at ab initio values.<sup>26</sup> Smaller multipole moments tend to lead to fewer problems at close range, where the

**Table 1.** Comparison of GDMA Multipole Moments and ESP-Fitted Multipole Moments for the Same Molecular Orientation of H<sub>2</sub>O<sup>a</sup>

	GDMA			fitted		
	H <sub>1</sub>	O	H <sub>2</sub>	H <sub>1</sub>	O	H <sub>2</sub>
Q <sub>00</sub>	0.488	−0.976	0.488	0.379	−0.758	0.379
Q <sub>11c</sub>	0.060	0.0	−0.060	0.010	0.0	−0.010
Q <sub>11s</sub>	−0.033	0.417	−0.033	−0.008	0.127	−0.008
Q <sub>20</sub>	−0.004	−0.020	−0.004	−0.035	−0.513	−0.035
Q <sub>22c</sub>	−0.001	0.132	−0.001	0.055	0.329	0.055
Q <sub>22s</sub>	0.017	0.0	−0.017	0.001	0.0	−0.001

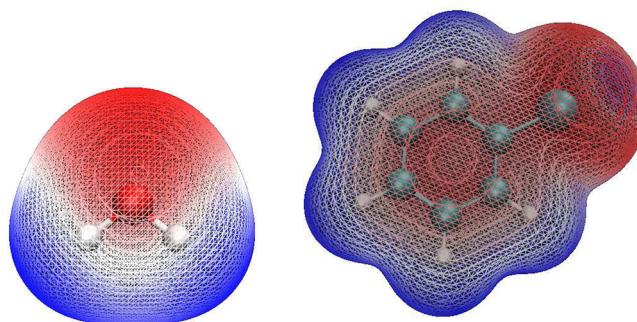
<sup>a</sup>All values are in au, components that are zero for all atoms are not shown.

multipole expansion is in error from the exact Coulomb integral by the so-called “penetration” correction.<sup>34,46</sup> Fitting without these constraints can also lead to large multipole moments that cancel one another to give accurate results for one geometry, but that lead to large errors after conformational change. Finally, so-called “buried” atoms, which lie within a molecule away from the molecular surface, can also take on unphysically large values during fitting as their contribution to the ESP at the molecular surface is small.<sup>31,47</sup> Constraining multipole moments toward zero alleviates this problem as interior atoms will be assigned very small charges.

Comparison of the ESP generated from the fitted multipole moments with B3LYP reference values across the entire volume of a finer grid with 429972 points outside the the 0.001 au isodensity surface yields a mean absolute error (MAE) of 0.37 kcal/mol. In the volume closest to the molecular surface (between the molecular 0.001 au isodensity surface and a surface 1.66 times further from the nuclei, “region A”),<sup>48</sup> the MAE is 0.61 kcal/mol. In “region B”, the volume between this surface and a surface 2.2 times the distance from the nuclei to the 0.001 au surface, the MAE is 0.04 kcal/mol. The corresponding MAEs using the GDMA multipole moments from Table 1 are larger at 0.64, 0.98, and 0.19 kcal/mol, respectively. Although alternative GDMA multipole moments can be found by trialing different integration radii,<sup>25</sup> there does not appear to be a systematic method for determining optimal radii for a given molecule.

The same approach was used for chlorobenzene, again applying symmetry constraints on individual multipole moment components during fitting across the volume of a sparse 3D grid with 2360 points outside the 0.001 au isodensity surface of the molecule. The MAE for the fitted multipole moments with respect to B3LYP reference data across a finer grid of 443275 points was found to be 0.28 kcal/mol. In region A closest to the molecular surface (defined above), the MAE is 0.84 kcal/mol, and in region B, the MAE reduces to 0.10 kcal/mol. For comparison purposes, a default GDMA analysis (no integration radii specified) yields a MAE of 0.65 kcal/mol across the entire grid, 1.82 kcal/mol for region A, and 0.31 kcal/mol for region B. As illustrated in Figure 5, the Cl atom of chlorobenzene exhibits a negative ring in the ESP orthogonal to the C–Cl bond, and a region of positive electrostatic potential at the surface along the C–Cl bond vector. This feature can be well-described using multipolar electrostatics but not using a single point charge at the Cl nuclear position.<sup>49,50</sup> The values of fitted atomic multipole moments for each atom are included as Supporting Information.

**DCM Charges.** H<sub>2</sub>O DCM charges for the fitted multipoles in Table 1 are presented in Table 2. An octahedral model (Figure 1,

**Figure 5.** DFT electrostatic potential energy mapped onto H<sub>2</sub>O 0.001 au isodensity surface (left) and chlorobenzene 0.001 au isodensity surface (right). Colors pass from positive ESP values (blue) through white to negative values (red).**Table 2.** Comparison of DCM Charges Representing the Same Underlying Multipole Expansion for the O-Atom in H<sub>2</sub>O<sup>a</sup>

charge (au)	DCM <sub>oct</sub>	charge (au)	DCM <sub>pyr</sub>
$q(d_q,0,0)$	2.76	$q(d_q,0,0)$	0.98
$q(-d_q,0,0)$	2.76	$q(-d_q,0,0)$	0.98
$q(0,d_q,0)$	−2.86	$q(0,d_q,0)$	0.0
$q(0,-d_q,0)$	−2.86	$q(0,0,0)$	−3.61
$q(0,0,d_q)$	−0.03	$q(0,0,d_q)$	0.55
$q(0,0,-d_q)$	−0.53	$q(0,0,-d_q)$	0.34

<sup>a</sup>The first DCM charges are arranged octahedrally with no central charge, the second set of DCM charges are arranged pyramidally (Figure 1). Labels represent the coordinates of the charges along the principal axes (eqs 2 and 3); all charges are 0.25  $a_0$  from the nuclear coordinates in the octahedral case, 0.6  $a_0$  from the nucleus in the pyramidal case.

right) with charges at a distance of 0.25  $a_0$  from nuclear coordinates ( $d_q = 0.25 a_0$  in eq 3) and a pyramidal model (eq 2) with charges at a distance of 0.6  $a_0$  from the O-nuclear positions and 0.25  $a_0$  from the H-nuclear positions were used. The larger distance for oxygen charges was chosen as the pyramidal model produces significantly larger charges than the octahedral model, which can be reduced by increasing  $d_q$ . It should be noted, however, that large charges cancel one another to yield the same total atomic charge as was present in the underlying multipole expansion.

As confirmed in Table 3, the DCM charges reproduce the multipole expansion exactly up to the truncation rank of  $l = 2$

**Table 3.** Comparison of Original Multipole Moments from Fitting to the ESP, Multipole Moments Calculated from DCM Charges in an Octahedral Arrangement,  $d_q = 0.25 a_0$  (eq 3), and from DCM Charges in a Pyramidal Arrangement,  $d_q = 0.6 a_0$  (eq 2), for the O-Atom of H<sub>2</sub>O<sup>a</sup>

component	multipole	DCM <sub>oct</sub>	DCM <sub>pyr</sub>
Q <sub>00</sub>	−0.758	−0.758	−0.758
Q <sub>11s</sub>	0.127	0.127	0.127
Q <sub>20</sub>	−0.513	−0.513	−0.513
Q <sub>22c</sub>	0.329	0.329	0.329
Q <sub>31s</sub>	0.0	−0.005	−0.028
Q <sub>33s</sub>	0.0	−0.006	−0.036

<sup>a</sup>All values are in au. Components not shown are equal to zero for all models. Multipoles were recalculated from the DCM charge distributions according to eq 1.



(quadrupole moment). As expected, there are nonzero octupole components arising from the point charge distribution, but by choosing a small value for  $d_q$  they are kept negligibly small. Even for the larger value of  $d_q = 0.6 a_0$ , the largest octupole component is  $-0.036$  au. As a final check, the same 3D grid outside the 0.001 au isodensity surface of the molecule used for multipole fitting was used to compare the ESP generated by DCM charges and multipole moments. A mean absolute difference between the full volume of the two grids of 0.03 kcal/mol was obtained, with 0.04 kcal/mol in region A. The maximum deviation between the pyramidal DCM and multipolar ESP across the entire grid was 0.5 kcal/mol. In the case of the octahedral DCM arrangement, the octupole is smaller than in the pyramidal arrangement, and the maximum deviation was 0.05 kcal/mol.

Larger charges were obtained using an octahedral model for chlorobenzene, reaching nearly 12 au for the Cl atom when  $d_q = 0.25 a_0$ . The behavior of the charges and octupole moment as a function of  $d_q$  were therefore examined in more detail (Table 4).

**Table 4. Properties of the Octahedral DCM Arrangement as a Function of  $d_q$  (eq 2, Right Hand Side of Figure 1) for Chlorobenzene<sup>a</sup>**

	$d_q = 0.25 a_0$	$d_q = 0.35 a_0$	$d_q = 0.45 a_0$	$d_q = 0.55 a_0$
mean abs. $q$	3.07	1.57	0.95	0.64
max. abs. $q$	11.67	6.09	3.77	2.58
mean abs. $Q_{3m}$	0.02	0.03	0.04	0.05
max. abs. $Q_{3m}$	0.20	0.28	0.36	0.44
ESP MAE	0.01	0.02	0.04	0.05
ESP Reg.A MAE	0.03	0.06	0.10	0.14
ESP Reg.A max.	0.54	1.06	1.73	2.57

<sup>a</sup>All charges and octupoles are in au; energies are kcal/mol. The mean absolute DCM charge and maximum DCM charge for any of the atoms is compared, along with mean and maximum octupole components. ESP MAE shows the impact of increasing  $d_q$  on the MAE of the ESP across the entire volume outside the 0.001 au surface of the molecule relative to a truncated multipole expansion ( $l = 2$ ). ESP Reg. A MAE is the MAE across region A closest to the molecule (defined in text) relative to a truncated multipole expansion, and ESP Reg.A max. shows the maximum difference across this region.

As shown in the Table, increasing  $d_q$  from 0.25 to  $0.55 a_0$  leads to a large decrease in the magnitude of DCM charges, with the largest charge in chlorobenzene dropping from 11.7 to 2.6 au. The corresponding increase in octupole moment is moderate, with a mean increase of 0.03 au in the individual components and a maximum increase of 0.24 au. This increase translates to an increase in the mean absolute discrepancy between multipole results and DCM results from 0.01 to 0.05 kcal/mol across the entire grid outside the 0.001 au isodensity surface of the molecule. In region A, closest to the molecule, the discrepancy increases from 0.03 to 0.14 kcal/mol. The maximum difference at any point on the grid increases from 0.5 to 2.6 kcal/mol, at a position lying on the molecular surface.  $d_q$  can therefore be used to control the magnitude of DCM charges with only a small effect on the ESP around a molecule. There is no need to use the same value of  $d_q$  for all atoms, so it can be selectively increased for problem atoms. It should also be emphasized that the increase in octupole moment can actually improve, rather than degrade accuracy relative to ab initio data, depending on the system, as truncation of the multipole expansion at quadrupole ignores the octupole moment contribution altogether.

**H<sub>2</sub>O Simulations.** Test simulations were performed to examine the stability of the DCM model in a Molecular Dynamics

context. Various existing multipolar approaches employ techniques such as rigid body approximations to simplify axis system derivatives,<sup>29</sup> which leads to small errors in the calculated forces, requiring constraints such as SHAKE, unphysically large bond force constants and/or very small simulation time steps. The focus in the following section is therefore to demonstrate that the current DCM implementation is appropriate for NVE molecular dynamics simulations with many time steps, no geometric constraints are required, a standard time step can be used, and simulations are stable even without distance cut-offs for the non-bonded terms, meaning that all charge–charge interactions are included for the entire system. Finally, stability of simulations with the maximum number of DCM charges required per atom and deliberately using large DCM charge values was tested. Simulations with the widely used TIP3P and CHARMM22 charge models were used to provide a reference in each case.

The first test system examined was the water trimer shown in Figure 6. 500 ps NVE simulations (500 000 time steps) at 50 K

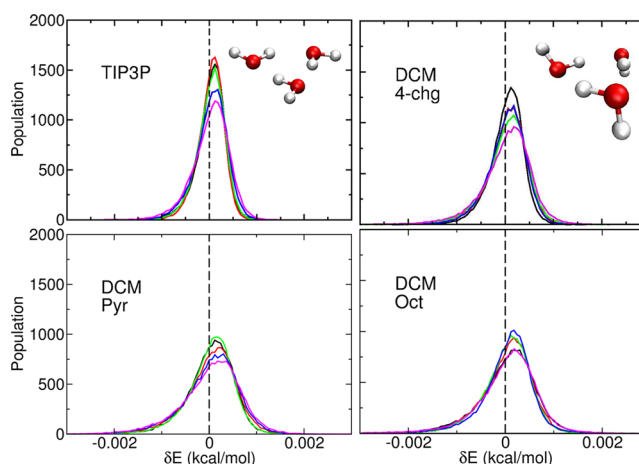


**Figure 6.** Normalized total energy distribution (kcal/mol) centered at the mean total energy for 500 ps NVE simulations of the H<sub>2</sub>O trimer at 50 K. Total energy is sampled every 10th time step (i.e., every 10 fs). No SHAKE constraints were applied, the different electrostatic models compared are TIP3P (top left), 4 DCM charges for O atoms (top-right), a pyramidal DCM charge arrangement (bottom-left) and an octahedral DCM arrangement (bottom-right). Energy distributions are shown for five separate simulations (different colors in the figure) for each charge model. Inset top-left: Snapshot taken from a TIP3P simulation showing the planar water geometry produced. Inset top-right: Snapshot of the geometry obtained using the DCM models.

demonstrated excellent energy conservation for all DCM charge models tested and stability of the cluster in its known minimum energy conformation.<sup>51</sup> As previously observed, running the simulation with isotropic charges from the widely used TIP3P model leads to a trimer geometry with all H and O atoms lying within a plane (top-left in the figure).<sup>6</sup> SHAKE constraints were not found to be necessary for energy conservation, despite the relatively large 1 fs time step for describing the O–H bonds. Although all charge models perform well, it can be seen that the standard TIP3P model used in CHARMM exhibits the smallest peak widths for the five simulations that were performed, indicating the lowest change in total energy per simulation time step and hence the greatest stability. There is little difference between the DCM models, although the four-charge model appears to exhibit slightly less variation than the two six-charge models, presumably due to the smaller number of charge–charge DCM interactions.



In addition, a comparison of analytically and numerically evaluated forces with respect to the  $x$ -,  $y$ -, and  $z$ -coordinate of each atom (often used in CHARMM to assess the precision of implemented analytical derivatives) demonstrates a maximum deviation of  $7 \times 10^{-4}$  kcal/mol·Å. Finally, electrostatic interaction energies were evaluated for the 10 diverse water dimers of Tschumper et al.<sup>52</sup> presented in Figure 7. As shown in Table 5

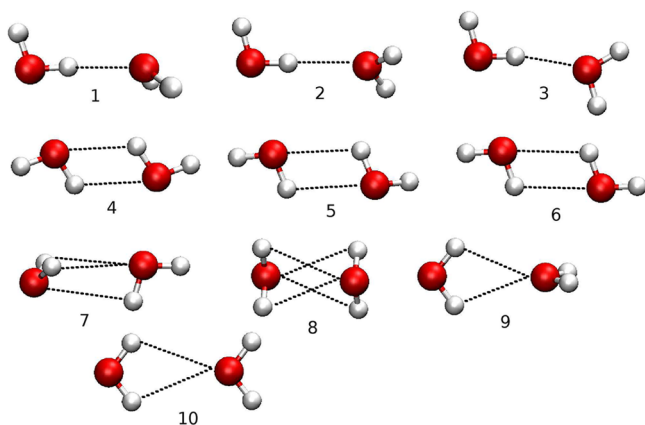


**Figure 7.** Ten water dimers of Tschumper et al.<sup>52</sup> used to compare the electrostatic interaction energy using different DCM models and multipole moments.

and Figure 8, there is excellent agreement between the octahedral and pyramidal DCM models with the fitted multipole moments that they are calculated from ( $r^2 = 1.00$ ). Similar agreement is observed between the four-charge model and the multipole expansion from which it is calculated. The one noticeable exception is for dimer 5, where electrostatic interaction energies from DCM charges differ from the corresponding multipole expansion by 0.28 kcal for the pyramidal model, and 0.59 kcal/mol for the four-charge model. As noted earlier, the four-charge model exhibits a larger octupole moment than the octahedral model, perhaps explaining the greater deviation from multipole results at close range. Good agreement is also observed between the DCM or multipolar results and the RVS Coulomb energy, both with  $r^2 = 0.99$ . The systematic underestimation of the electrostatic interaction energy with respect to RVS data by both DCM charges and multipole moments may be partially due to the difference in level of theory (RVS data is only available for RHF, whereas multipoles for the DCM charges were calculated using

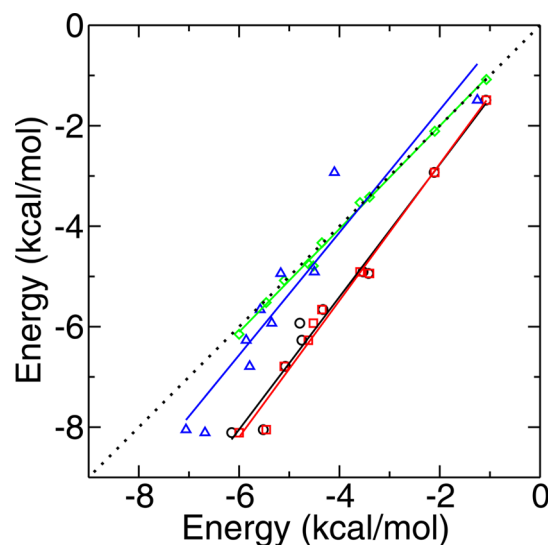


**Figure 8.** Comparison of DCM octahedral charge model vs multipolar electrostatic interaction energy for 10 water dimers (green diamonds,  $r^2 = 1.00$ ), DCM octahedral model electrostatic interaction energy vs RVS aug-cc-pVQZ Coulomb energy (red squares,  $r^2 = 0.99$ ), multipolar energy vs RVS Coulomb energy (black circles,  $r^2 = 0.99$ ) and TIP3P electrostatic interaction energy vs RVS Coulomb energy (blue triangles,  $r^2 = 0.95$ ). Electrostatic interaction energies are in kcal/mol.

B3LYP electric fields), but it is likely to be largely due to the absence of a “penetration” correction term, which becomes important at close-range,<sup>53</sup> and to truncation of the multipole expansion at quadrupole. TIP3P data are also included for comparison, and while electrostatic interaction energies are larger than for DCM charges, reducing the systematic error, the larger spread ( $r^2 = 0.95$ ) affects the model’s ability to correctly rank the relative energies of the different dimers.

A similar test was performed for a low-energy water trimer geometry (top right-hand side of Figure 6) using the fitted multipoles, the octahedral and the pyramidal DCM charge arrangements. From a total electrostatic interaction energy of  $-23.2$  kcal/mol, a maximum difference of 0.03 kcal/mol was observed between all 3 models. For the four-charge model a lower interaction energy of  $-20.2$  kcal/mol was obtained with a total discrepancy of 0.2 kcal/mol from the corresponding multipole expansion. There is therefore little impact on the electrostatic interaction energy upon changing from multipoles to DCM

**Table 5.** Electrostatic Interaction Energies (kcal/mol) for 10 Water Dimers<sup>52</sup> Using the DCM Octahedral (DCM<sub>Oct</sub>) and Pyramidal (DCM<sub>Pyr</sub>) Models, Compared with TIP3P, Results Using the Fitted Multipole Expansion (MTP) from which the Models Were Derived and the RVS Energy Decomposition Coulomb Term at the RHF/aug-cc-pVQZ Level of Theory<sup>a</sup>

	DCM <sub>Oct</sub>	DCM <sub>Pyr</sub>	MTP	TIP3P	RVS	DCM <sub>4chg</sub>	MTP <sub>L</sub>
dimer 1	−6.00	−6.00	−6.15	−6.68	−8.11	−5.73	−5.70
dimer 2	−4.62	−4.62	−4.75	−5.86	−6.27	−4.14	−4.08
dimer 3	−5.46	−5.46	−5.52	−7.06	−8.05	−4.47	−4.40
dimer 4	−5.10	−5.10	−5.08	−5.79	−6.79	−4.35	−4.25
dimer 5	−4.52	−4.51	−4.79	−5.35	−5.93	−3.02	−3.61
dimer 6	−4.35	−4.35	−4.33	−5.58	−5.66	−2.60	−2.52
dimer 7	−3.59	−3.59	−3.53	−4.50	−4.91	−3.74	−3.49
dimer 8	−1.07	−1.07	−1.08	−1.25	−1.49	−1.38	−1.40
dimer 9	−3.40	−3.40	−3.42	−5.17	−4.94	−4.13	−4.18
dimer 10	−2.10	−2.10	−2.11	−4.10	−2.93	−2.48	−2.51

<sup>a</sup>A similar comparison on the right hand side of the table compares the four-charge DCM model (DCM<sub>4chg</sub>) with the compact multipolar model of Lee et al.<sup>36</sup> (MTP<sub>L</sub>) to which it corresponds.

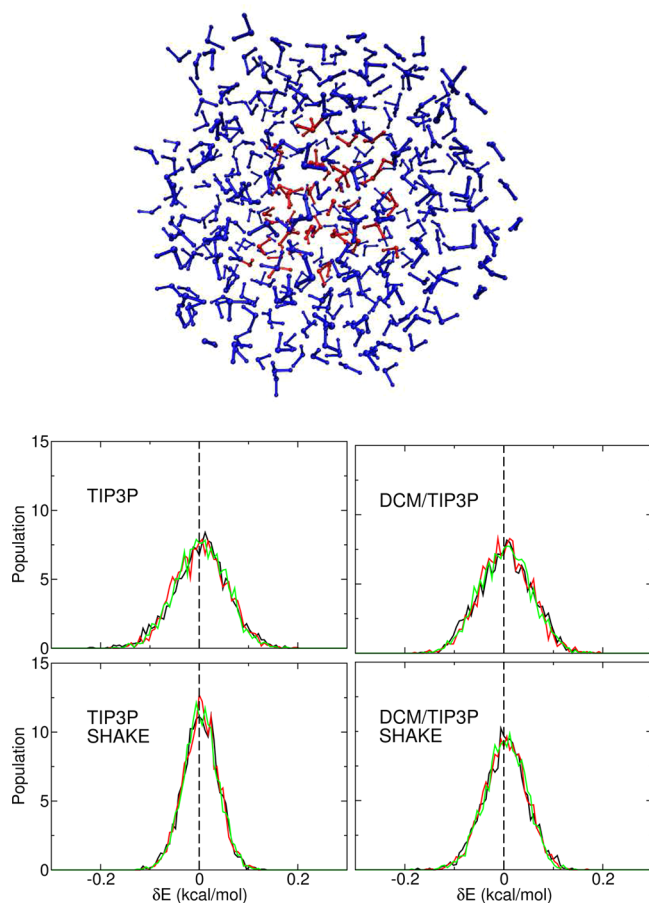


**Figure 9.** Top: Snapshot taken from a 75 ps (300 000 time step) NVE mixed DCM/TIP3P H<sub>2</sub>O droplet MD simulation. DCM molecules are shown in red, TIP3P molecules are blue. Middle: Normalized total droplet energy distribution (kcal/mol) centered at the average value recorded during each trajectory, written every 100th time step for three separate trajectories (different colors). No SHAKE constraints were applied. TIP3P results are shown on the left, a four-charge DCM arrangement was used for O atoms of inner-shell molecules in the model on the right. Bottom: As for middle but for 300 ps trajectories with SHAKE constraints and a 1 fs time step.

charges, compared with the much greater impact of changing between different multipolar models.

Next, a larger water droplet (Figure 9) containing 369 molecules was examined as a more realistic system and as an example of a split level TIP3P/DCM calculation with an inner core of DCM water molecules and an outer shell of TIP3P molecules. Using this approach, a region of interest such as a protein binding site can be treated in detail while the remainder of the system is treated with a coarser force field representation. As shown in the center-right part of the figure, over three 75 ps simulations the TIP3P/DCM model remains stable. There is no visible energy drift and the distribution of the total energy (kinetic + potential energy) is largely within 0.25 kcal/mol despite a total electrostatic interaction energy of around 4500 kcal/mol for the entire system. For comparison purposes, the same simulation conditions were used after replacing the inner DCM core with additional TIP3P water molecules. As seen in the center-left-hand side of the figure, the energy distribution using a fully TIP3P model does not differ significantly from DCM results. The same conclusions were found to apply when SHAKE constraints are used for H atoms with a longer, 1 fs time step in

300 ps simulations, as shown in the bottom part of the figure, although there is perhaps some broadening of the total energy distribution relative to TIP3P data.

The computational cost of running DCM simulations as a function of the charge model chosen was then examined by benchmarking simulations of a smaller water droplet containing 130 molecules with a spherical restraining potential (Table 6).

**Table 6. Benchmarking of 3000 Time Steps on One Core of an Intel i7 3.20 GHz Processor for a Water Droplet System as a Function of the Charge Model Used<sup>a</sup>**

	TIP3P	DCM-TIP3P	DCM (4-charge)	DCM (pyramidal)	DCM (octahedral)
time (s)	6.3	12.5	50.8	422.3	460.8

<sup>a</sup>CPU times (s) are averaged over 5 runs in each case.

On a 3.20 GHz Intel i7 processor using a single core the standard CHARMM program with TIP3P water model proceeds quickly, completing 3000 simulation time steps in 6.3 s. This includes the time required to evaluate all other bonded and nonbonded energy terms, and to propagate the simulation.

Running the same simulation with the same TIP3P model and the new DCM code (labeled TIP3P-DCM in Table 6) increases the CPU time to 12.5 s. The difference can be ascribed to a combination of code optimization in CHARMM, and to the time spent evaluating eqs 15–23 for each frame. Although these terms are not necessary in frames where all charges are placed at nuclear positions, they are evaluated here for analysis purposes. These terms therefore require maximally 6 s, in this case, roughly doubling the total simulation time.

The same number of these terms is required for the octahedral charge arrangement with six DCM charges, but as shown in the table, the total CPU time required for this model increases dramatically to 460.8 s. This is roughly in line with the prediction of scaling with  $n^2 t_d$  described above, where the octahedral model is expected to be  $36 t_d$  times slower than the TIP3P-DCM model with  $t_d > 1$ .

Moving one of the six charges to the nuclear coordinate, creating the pyramidal charge arrangement, reduces the simulation time to 422.3 s. This is clearly a non-negligible improvement for no loss of accuracy, confirming that the nuclear position should be occupied by one DCM charge wherever possible. Also, if the time saving per charge that is shifted to the nuclear coordinate is estimated from Table 6 to be 38 s, then the computational cost of using off-centered charges can be estimated using a hypothetical arrangement with all six charges shifted to the origin, which yields an expected total simulation time of 232 s ( $460 - 38 \times 6$ ), or roughly 50% of the octahedral value. The use of off-centered charges, requiring the terms in eqs 12–14, therefore roughly doubles computational cost of the electrostatic term, that is, in  $n^2 t_d$ ,  $t_d \approx 2$  for the current implementation.

Reducing the number of oxygen DCM charges to 4, with a single charge on each H atom has the strongest impact, reducing the simulation time to 50.8 s. Of all the improvements that can be made to improve computational efficiency, reducing the required number of DCM charges is therefore most important. Future development of the method should therefore focus on finding minimal charge arrangements that yield a required level of accuracy in the electrostatic interaction energy.

Finally, simulations were run for chlorobenzene in a droplet of 171 water molecules (Figure 10). As demonstrated in Table 2, DCM charges can be considerably larger than standard force field

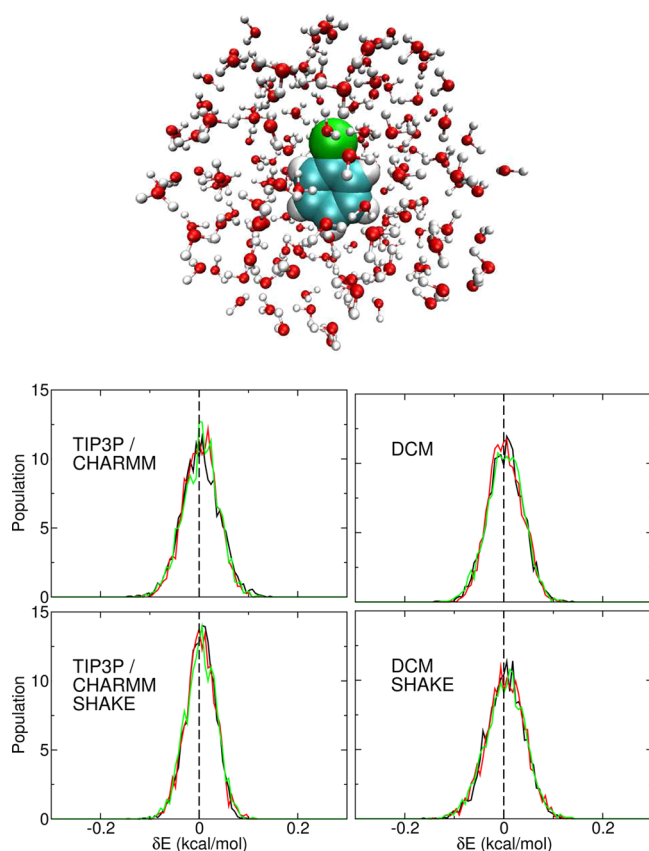


**Figure 10.** Top: Snapshot taken from a 75 ps (300000 time step) NVE DCM solvated chlorobenzene MD simulation. Middle: Normalized distribution of total system energy centered at mean (kcal/mol), written every 100th time step. No SHAKE constraints were applied, either TIP3P plus CHARMM22 (left) or a pyramidal DCM charge arrangement (right) was used for all atoms. Three trajectories are shown in each case (different colors). Bottom: As for middle, but taken from 300 ps simulations using SHAKE with a 1 fs time step.

point charges if small  $d_q$  values are chosen. Charge magnitudes can be decreased by increasing  $d_q$ , but at the cost of increasing the atomic octupole moment, which may in some cases be undesirable. Unlike in a standard point-charge force field, however, DCM charges are balanced by neighboring charges that are a comparatively short distance away, meaning that the total atom–atom interaction energy and forces are the same as when using a multipole expansion (again, when  $d_q$  is small). It is therefore important to ascertain whether simulations involving such large individual charges are stable under standard simulation conditions. To this end, DCM models were chosen for  $H_2O$  and chlorobenzene with up to 6 charges per atom, the largest number of charges that is likely to be used in a quadrupolar DCM simulation, in combination with very large DCM charge values by usual force field standards. The pyramidal charge model was applied to all water and chlorobenzene atoms, with a relatively small  $d_q$  value of  $0.25 a_0$  (eq 2) so that individual charges reached 25 au for Cl and 3 au for oxygen in  $H_2O$ . All charges and their coordinates are provided in the Supporting Information. Smaller charges were possible using different charge arrangements, and as shown in Table 4 charges can be reduced significantly in chlorobenzene by increasing  $d_q$  with little impact on atomic octupole moments, but it is instructive to examine the stability of a “worst case scenario”. It is therefore encouraging that trajectories remain comparable to corresponding TIP3P simulations in terms of

energy conservation and total energy distribution (center and bottom of Figure 10). The presence of counterbalancing charges in close proximity to each large DCM charge position can therefore yield an accurate total energy without significant loss of precision.

**Compact Charge Models.** The above results demonstrate that DCM simulations are stable with respect to the number of charges  $n$  per atom, tested up to  $n = 6$ , and with respect to the magnitude of these charges as tested up to 25 au. Accuracy is the same as for a standard multipolar simulation if  $d_q$  is kept small, with little loss of precision up to  $d_q = 0.55 a_0$  and with the potential for increased accuracy relative to a truncated multipole expansion if  $d_q$  is exploited to control the atomic octupole moment. Finally, it was shown that the computational cost, and therefore range of applicability, of DCM simulations, is heavily dependent on the number of DCM charges used per atom. With this in mind, it is important to search for DCM models with a reduced number of charges that might still exactly reproduce multipole moments up to the truncation rank.

The approach used here is to exploit  $d_q$  more fully, as in eqs 5 and 6 (also expanded in section S4 of the Supporting Information). A similar system of six simultaneous equations was therefore created to express the multipoles  $Q_{lm}$  for an arrangement of four charges at  $(d_1, 0, 0)$ ,  $(0, d_2, 0)$ ,  $(0, 0, d_3)$ , and  $(0, 0, 0)$ , which was solved as before to yield expressions for the four charges and two distances  $d_1$  and  $d_3$  in terms of the multipole moments.  $d_2$  can be fixed by the user. The six simultaneous equations yield the following solutions:

$$q_{(d_1, 0, 0)} = \frac{Q_{11c}^2}{d_2 Q_{11s} + \frac{2}{3} \sqrt{3} Q_{22c}} \quad (34)$$

$$q_{(0, d_2, 0)} = \frac{Q_{11s}}{d_2} \quad (35)$$

$$q_{(0, 0, d_3)} = \frac{\sqrt{3} Q_{10}^2}{\sqrt{3} d_2 Q_{11s} + \sqrt{3} Q_{20} + Q_{22c}} \quad (36)$$

$$q_{(0, 0, 0)} = Q_{00} - \sum_{i=1}^3 q_i \quad (37)$$

$$d_1 = \frac{d_2 Q_{11s} + \frac{2}{3} \sqrt{3} Q_{22c}}{Q_{11c}} \quad (38)$$

$$d_3 = \frac{d_2 Q_{11s} + Q_{20} + \frac{1}{\sqrt{3}} Q_{22c}}{Q_{10}} \quad (39)$$

In the case of six nonzero multipole components remaining after diagonalization of the quadrupole tensor, this arrangement of four charges yields the same multipole moments up to quadrupole as a multipole expansion with six terms, or as the arrangements in eqs 2 and 3 with 6 charges. Unlike the DCM models with six charges, however, the range of applicability of this model is restricted to systems where all multipole terms that appear in the denominators of eqs 34–39 are nonzero, and also to values of the multipole moments that do not cause excessively large values of  $d_1$  and  $d_3$ . The clear advantage of the model is a more than 2-fold decrease in the computational cost when compared to a 6-pt charge model.

## PERSPECTIVES

The DCM method presented here is substantially simpler in its implementation than a standard multipolar approach due to the



homogeneity of the terms involved. As such, and as each term in the electrostatic interaction energy is a standard point-charge Coulomb interaction, the method should lend itself well to integration with standard MD techniques such as periodic boundaries and Ewald summation, and as already shown,<sup>22</sup> the DCM model can be interfaced with QM code for multipolar QM/MM calculations.

For sensitive applications, extension to higher interaction ranks (octupole moments and beyond) would require the selection of an arrangement with the appropriate number of charges. A fully octupolar implementation for an atom with all multipole moments nonzero should therefore require maximally seven additional charges for the seven additional spherical multipole moment terms.

In much the same way that molecular symmetry causes certain atomic multipole moments to vanish, decreasing the number of multipole–multipole interaction terms that need to be evaluated,<sup>29</sup> DCM models can be developed with fewer than 6 charges. An exhaustive list of models for each atomic symmetry is being implemented into a single tool to automatically select the most efficient DCM arrangement for a given atom, providing charges for use in CHARMM.

The current implementation of DCM does not allow charges to fluctuate as a function of molecular geometry. Intramolecular polarization could therefore only be encapsulated in an average way by fitting optimal multipole moments to the ESP of a molecule in many different conformations. A more rigorous extension would allow DCM charges to fluctuate as a function of nuclear coordinates.<sup>54,55</sup>

Finally, work has so far focused on equivalence with a standard multipolar approach. There is much scope, however, to fit arbitrary atomic charge arrangements directly to the ESP in order to increase accuracy or decrease the number of charges required. Similar studies have been performed for static charge arrangements<sup>56</sup> or rigid molecules<sup>57,58</sup> in the past, and the framework introduced here allows application of this approach in a dynamic, conformationally evolving system and for systems beyond water.

## SUMMARY

The Distributed Charge Model (DCM) described here is a novel and computationally efficient multipolar electrostatics implementation for MD simulations. Inspired by the recent octahedral point charge arrangement of Gao and co-workers used in Fragment Molecular Orbital calculations, the approach has been optimized using a spherical harmonics representation to reduce the maximum number of nonzero multipole components to six, and by exploiting symmetric environments with further vanishing multipole components to reduce the number of required charges further. A framework has been introduced to define charge positions relative to surrounding nuclei in order to distribute torques throughout a molecule in MD simulations. The implementation has been validated in test simulations with CHARMM, demonstrating equivalence with a standard multipole expansion, energy conservation during NVE simulations without the need for short time steps or SHAKE constraints, and computational efficiency of the underlying algorithm.

The DCM approach is relatively straightforward to implement into existing MD code due to the homogeneity of the terms involved. Extension to periodic boundary conditions and Ewald summation is underway. The use of distributed charges rather than point multipoles also allows interfacing with Quantum Chemical (QM) code for multipolar QM/MM-MD simulations without modification of the underlying QM software. As a future

development, the same framework can be used for optimal charge arrangements that are fitted directly to the electrostatic potential energy and not designed to represent multipole moments, allowing increased accuracy and/or a smaller number of charges per atom.

## ASSOCIATED CONTENT

### Supporting Information

Sample DCM charges and their coordinates, along with the atomic multipole moments used to calculate them. Expanded workings showing how expressions are derived for different charge arrangements. This material is available free of charge via the Internet at <http://pubs.acs.org/>.

## AUTHOR INFORMATION

### Corresponding Author

\*Phone: +41 61 267 38 21. Fax: +41 61 267 38 55. Email: [m.meuwly@unibas.ch](mailto:m.meuwly@unibas.ch).

### Notes

The authors declare no competing financial interest.

## ACKNOWLEDGMENTS

The work has been partially supported by the Swiss National Science Foundation (Grant 200021-117810) and the NCCR MUST. D.G.F. was supported by the Next Generation Super Computing Project, Nanoscience Program (MEXT, Japan), and Computational Materials Science Initiative (CMSI, Japan).

## REFERENCES

- (1) Buckingham, A. D.; Fowler, P. W. *J. Chem. Phys.* **1983**, *79*, 6426–6428.
- (2) Day, P. N.; Jensen, J. H.; Gordon, M. S.; Webb, S. P.; Stevens, W. J.; Krauss, M.; Garmer, D.; Basch, H.; Cohen, D. J. *J. Chem. Phys.* **1996**, *105*, 1968–1986.
- (3) Gresh, N.; Claverie, P.; Pullman, A. *Theor. Chim. Acta* **1984**, *66*, 1–20.
- (4) Sokalski, W. A.; Poirier, R. A. *Chem. Phys. Lett.* **1983**, *98*, 86–92.
- (5) Engkvist, O.; Åstrand, P.-O.; Karlström, G. *Chem. Rev.* **2000**, *100*, 4087–4108.
- (6) Shaik, M.; Devereux, M.; Popelier, P. *Mol. Phys.* **2008**, *106*, 1495–1510.
- (7) Plattner, N.; Meuwly, M. *Biophys. J.* **2008**, *94*, 2505–2515.
- (8) Karamertzanis, P. G.; Price, S. L. *J. Chem. Theory Comp.* **2006**, *2*, 1184–1199.
- (9) Devereux, M.; Plattner, N.; Meuwly, M. *J. Phys. Chem. A* **2009**, *113*, 13199–13209.
- (10) Zheng, X.; Wu, C.; Ponder, J. W.; Marshall, G. R. *J. Am. Chem. Soc.* **2012**, *134*, 15970–15978.
- (11) Lee, M. W.; Meuwly, M. *J. Phys. Chem. A* **2011**, *115*, 5053.
- (12) Lee, M. W.; Carr, J. K.; Goellner, M.; Hamm, P.; Meuwly, M. *J. Chem. Phys.* **2013**, *139*, 54506.
- (13) Lee, M. W.; Meuwly, M. *J. Phys. Chem. Chem. Phys.* **2013**, *15*, 20303.
- (14) Liem, S.; Popelier, P. *J. Chem. Phys.* **2003**, *119*, 4560–4566.
- (15) Plattner, N.; Meuwly, M. *Biophys. J.* **2008**, *94*, 2505–2515.
- (16) Piquemal, J.-P.; Cisneros, G. A.; Reinhardt, P.; Gresh, N.; Darden, T. A. *J. Chem. Phys.* **2006**, *124*, 104101.
- (17) Weiner, S. J.; Kollman, P. A.; Case, D. A.; Singh, U.; Ghio, C.; Alagona, G.; Profeta, S., Jr; Weiner, P. *J. Am. Chem. Soc.* **1984**, *106*, 765–784.
- (18) MacKerell, A. D., Jr.; Bashford, D.; Bellott, M.; Dunbrack, J. R. L.; Evanseck, J. D.; Field, M. J.; Fischer, S.; Gao, J.; Guo, H.; Ha, S.; Joseph-McCarthy, D.; Kuchnir, L.; Kuczera, K.; Lau, F. T. K.; Mattos, C.; Michnick, S.; Ngo, T.; Nguyen, D. T.; Prodhom, B.; W. E. Reiher, I.; Roux, B.; Schlenkrich, M.; Smith, J. C.; Stote, R.; Straub, J.; Watanabe, M.; Wiorkiewicz-Kuczera, J.; Yin, D.; Karplus, M. *J. Phys. Chem. B* **1998**, *102*, 3586–3616.

- (19) Plattner, N.; Bandi, T.; Doll, J.; Freeman, D. L.; Meuwly, M. *Mol. Phys.* **2008**, *106*, 1675–1684.
- (20) Raval, A.; Piana, S.; Eastwood, M. P.; Dror, R. O.; Shaw, D. E. *Proteins* **2012**, *80*, 2071–2079.
- (21) Sawaryn, A.; Sokalski, W. A. *Comput. Phys. Commun.* **1989**, *52*, 397–408.
- (22) Gao, Q.; Yokojima, S.; Fedorov, D. G.; Kitaura, K.; Sakurai, M.; Nakamura, S. *Chem. Phys. Lett.* **2014**, *593*, 165–173.
- (23) Kitaura, K.; Ikeo, E.; Asada, T.; Nakano, T.; Uebayasi, M. *Chem. Phys. Lett.* **1999**, *313*, 701–706.
- (24) Bader, R. F. W. *Atoms in Molecules—A Quantum Theory*; Oxford University Press: Oxford, 1990.
- (25) Stone, A. J. *J. Chem. Theory Comp.* **2005**, *1*, 1128–1132.
- (26) Devereux, M.; Gresh, N.; Piquemal, J.-P.; Meuwly, M. *J. Comput. Chem.* **2014**, *35*, 1577–1591.
- (27) Kramer, C.; Gedeck, P.; Meuwly, M. *J. Comput. Chem.* **2012**, *33*, 1673–1688.
- (28) Bereau, T.; Kramer, C.; Monnard, F. W.; Nogueira, E. S.; Ward, T. R.; Meuwly, M. *J. Phys. Chem. B* **2007**, *117*, 5460.
- (29) Bereau, T.; Kramer, C.; Meuwly, M. *J. Chem. Theory Comp.* **2013**, *9*, 5450–5459.
- (30) Kramer, C.; Gedeck, P.; Meuwly, M. *J. Chem. Theory Comp.* **2013**, *9*, 1499.
- (31) Bayly, C. I.; Cieplak, P.; Cornell, W.; Kollman, P. A. *J. Phys. Chem.* **1993**, *40*, 10269–10280.
- (32) Wu, J. C.; Chattree, G.; Ren, P. *Theor. Chem. Acc.* **2012**, *131*, 1138.
- (33) Vigne-Maeder, F.; Claverie, P. *J. Chem. Phys.* **1988**, *88*, 4934–4948.
- (34) Stone, A. J. *The Theory of Intermolecular Forces*; Clarendon Press: Oxford, 1996.
- (35) Popelier, P. L. A. *Atoms in Molecules. An Introduction*; Pearson Education: London, 2000.
- (36) Lee, M. W.; Plattner, N.; Meuwly, M. *Phys. Chem. Chem. Phys.* **2012**, *14*, 15464–15474.
- (37) Ren, P.; Wu, C.; Ponder, J. W. *J. Chem. Theory Comp.* **2011**, *7*, 3143–3161.
- (38) van Gunsteren, W.; Berendsen, H. *Mol. Phys.* **1977**, *34*, 1311–1327.
- (39) Frisch, M. J.; Trucks, G. W.; Schlegel, H. B.; Scuseria, G. E.; Robb, M. A.; Cheeseman, J. R.; Scalmani, G.; Barone, V.; Mennucci, B.; Petersson, G. A.; Nakatsuji, H.; Caricato, M.; Li, X.; Hratchian, H. P.; Izmaylov, A. F.; Bloino, J.; Zheng, G.; Sonnenberg, J. L.; Hada, M.; Ehara, M.; Toyota, K.; Fukuda, R.; Hasegawa, J.; Ishida, M.; Nakajima, T.; Honda, Y.; Kitao, O.; Nakai, H.; Vreven, T.; Montgomery, J. A.; Jr.; Peralta, J. E.; Ogliaro, F.; Bearpark, M.; Heyd, J. J.; Brothers, E.; Kudin, K. N.; Staroverov, V. N.; Kobayashi, R.; Normand, J.; Raghavachari, K.; Rendell, A.; Burant, J. C.; Iyengar, S. S.; Tomasi, J.; Cossi, M.; Rega, N.; Millam, J. M.; Klene, M.; Knox, J. E.; Cross, J. B.; Bakken, V.; Adamo, C.; Jaramillo, J.; Gomperts, R.; Stratmann, R. E.; Yazyev, O.; Austin, A. J.; Cammi, R.; Pomelli, C.; Ochterski, J. W.; Martin, R. L.; Morokuma, K.; Zakrzewski, V. G.; Voth, G. A.; Salvador, P.; Dannenberg, J. J.; Dapprich, S.; Daniels, A. D.; Farkas, O.; Foresman, J. B.; Ortiz, J. V.; Cioslowski, J.; Fox, D. J. *Gaussian 09*, Revision A.02; Gaussian, Inc.: Wallingford, CT, 2009.
- (40) Law, M. M.; Hutson, J. M. *Comput. Phys. Commun.* **1997**, *102*, 252.
- (41) Stevens, W. J.; Fink, W. *Chem. Phys. Lett.* **1987**, *139*, 15–22.
- (42) Schmidt, M.; Baldrige, K.; Boatz, J.; Elbert, S.; Gordon, M.; Jensen, J.; Koseki, S.; Matsunaga, N.; Nguyen, K.; Su, S.; Windus, T.; Dupuis, M., Jr.; Montgomery, J. *J. Comput. Chem.* **1993**, *14*, 1347–1363.
- (43) Schuchardt, K.; Didier, B.; Elsethagen, T.; Sun, L.; Gurumoorathi, V.; Chase, J.; Li, J.; Windus, T. *J. Chem. Inf. Model.* **2007**, *47*, 1045–1052.
- (44) Jorgensen, W. L.; Chandrasekhar, J.; Madura, J. D.; Impey, R. W.; Klein, M. L. *J. Chem. Phys.* **1983**, *79*, 926–935.
- (45) Vanommeslaeghe, K.; Hatcher, E.; Acharya, C.; Kundu, S.; Zhong, S.; Shim, J.; Darian, E.; Guvench, O.; Lopes, P.; Vorobyov, I.; Mackerell, A. D., Jr. *J. Comput. Chem.* **2009**, *31*, 671–690.
- (46) Freitag, M. A.; Gordon, M. S.; Jensen, J. H.; Stevens, W. J. *J. Chem. Phys.* **2000**, *112*, 7300–7306.
- (47) Sigfridsson, E.; Ryde, U. *J. Comput. Chem.* **1998**, *19*, 377–395.
- (48) Richards, F. M.; Lee, B. *J. Mol. Biol.* **1971**, *55*, 379–400.
- (49) El Hage, K.; Piquemal, J.-P.; Hobaiika, Z.; Maroun, R. G.; Gresh, N. *J. Comput. Chem.* **2013**, *34*, 1125–1135.
- (50) Wilcken, R.; Zimmermann, M. O.; Lange, A.; Joerger, A. C.; Boeckler, F. M. *J. Med. Chem.* **2013**, *56*, 1363–1388.
- (51) Wales, D. J.; Hodges, M. P. *Chem. Phys. Lett.* **1998**, *286*, 65–72.
- (52) Tschumper, G. S.; Leininger, M. L.; Hoffman, B. C.; Valeev, E. F.; Schaefer, H. F.; Quack, M. *J. Chem. Phys.* **2002**, *116*, 690–701.
- (53) Piquemal, J.-P.; Gresh, N.; Giessner-Prettre, C. *J. Phys. Chem. A* **2003**, *107*, 10353–10359.
- (54) Mills, M. J. L.; Popelier, P. L. A. *Theor. Chem. Acc.* **2012**, *131*, 1137.
- (55) Nutt, D.; Meuwly, M. *Biophys. J.* **2003**, *85*, 3612–3623.
- (56) Karamertzanis, P. G.; Pantelides, C. C. *Mol. Sim.* **2004**, *30*, 413–436.
- (57) Mahoney, M. W.; Jorgensen, W. L. *J. Chem. Phys.* **2000**, *112*, 8910–8922.
- (58) Tröster, P.; Lorenzen, K.; Tavan, P. *J. Phys. Chem. B* **2014**, *118*, 1589–1602.